Aptamer Fiber Anchored on the Edge of a Protein Pattern: A Template for Nanowire Fabrication

Pei Gao and Yuguang Cai*

Department of Chemistry, University of Kentucky, 505 Rose Street, Lexington, Kentucky 40506

ARTICLE

ABSTRACT How to lay down nanowires at designated positions is a challenge that undermines the development of nanowire-based devices. We demonstrate that aptamer fibers, which are formed by the self-assembly of multiple aptamers, anchor specifically on the edge of protein patterns. This edge-anchoring effect originates from the biospecific recognition between the aptamer and its target protein. The fractal- shaped aptamer fibers are 1—6 nm high and can be tens of micrometers long. Once these edge-bound fibers have formed, they can serve as scaffolds for further assembly processes. We used these aptamer fibers as templates to fabricate palladium and streptavidin nanowires, which anchored on the pattern edges and never cross over or collapse over each other. The aptamer fiber scaffold provides a solution for fabricating and interfacing nanowires to existing surface patterns.

KEYWORDS: aptamer · fibers · palladium nanowire · Streptavidin nanowire · protein pattern · edge-binding effect · DNA scaffold · AFM

Nanowires have unique properties not seen in bulk materials.[1] Many proto-type applications like high performance solar cells, waveguides, nanolasers, nanotransistors, and biosensors are based on novel functions of nanowires.[2−5] Two technical challenges that undermine the development of nanowire-based devices are how to interface freestanding nanowires to the existing device on a solid substrate and how to control the positions of freestanding nanowires on a substrate. One approach to address these problems is to use lithographic patterns to control the position of nanowires. Nanowires can be directed to the lithographic patterns either standing up like trees in a forest,[5,6] or collapsing over the pattern.[7,8] However, in many applications, such as conductive wires connecting different electrodes, nanowire transistors, and nanowire memory switches,[9] nanowires are required to lay down on the surface. Furthermore, these wires must not cross or collapse over each other. Without manipulating nanowires individually, laying down nanowires at designated positions while avoiding overlapping remains a challenging task.

In this study, we report a deoxyribonucleic acid (DNA) nanotechnology approach to tackle the problem of interfacing and positioning nanowires. The DNA nanotechnology enables us to create complicated structures on surfaces.[10−13] Our approach employs the biospecific recognition of DNA aptamers. Aptamers are single-stranded nucleic acids, which specifically bind to their targets.[14−20] The aptamer-protein binding has been used to build supramolecular structures at nanoscale.[21,22] When an antilysozyme aptamer reacted with a lithographic pattern of lysozyme on the surface, the aptamer preferentially bound on the edge of the lysozyme pattern.[23] We found that, if the lysozyme pattern was incubated in concentrated aptamer solution and then in a buffer solution for a longer time, additional aptamers in the solution self-assembled into surface-bound aptamer fibers, one end of which anchored on the edge of the lysozyme pattern. Thus, a DNA scaffold was formed, which grew from the edge of the protein pattern. Nanowires anchored from the edges of surface patterns could be fabricated on the aptamer fiber template. As a result, these nanowires on the surface never crossed over each other. The biospecific recognition between the antilysozyme aptamer and lysozyme pattern determined that the nanowires fabricated from the aptamer fiber scaffold always initiated from the edge of the protein pattern. Therefore, our approach for the nanowire fabrication offers a means to attach and interface the nanowire to existing protein-coated patterns.

RESULTS AND DISCUSSIONS

Scheme 1 illustrates our experimental procedure. We prepared the cross-linked silane film (OTS film) on the hydroxyl-terminated

*Address correspondence to ycai3@uky.edu.

Received for review August 24, 2009 and accepted October 18, 2009.

Published online October 26, 2009.
10.1021/nn901082u CCC: $40.75

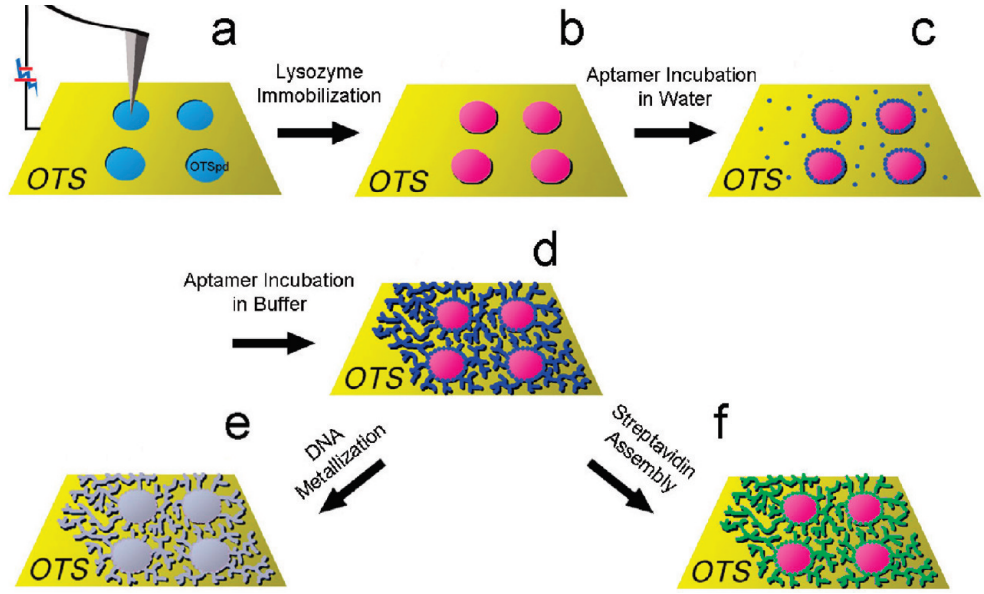

Scheme 1. (a) Fabrication of the carboxylic acid-terminated OTSpd pattern (light blue disks) on an OTS surface using the scanning probe deep oxidation lithography. (b) The OTSpd chemical pattern was incubated with a solution of lysozyme. A monolayer of tightly packed lysozyme formed on the OTSpd pattern. (pink disks). (c) Incubation of the lysozyme pattern with a solution of antilysozyme aptamer in water. The aptamers preferentially bound on the edge of the lysozyme disks and formed rings (dark blue rings). Additional aptamers nonspecifically adsorbed on the OTS surface. (dark blue dots). (d) Incubation of the lysozyme pattern with the antilysozyme aptamer in a 10 mM Tris buffer. The nonspecifically adsorbed aptamers self-assembled into fibers (dark blue wires in figure), which anchored on the edges of lysozyme patterns. (e) The aptamer fibers were converted into Pd nanowires (silver wires in figure) through DNA metallization. In the mean time, the lysozyme patterns were also coated with a layer of Pd (silver disks in figure). (f) Streptavidin (green) assembled on the fibers made of biotin-tagged aptamers.

silicon (100) surface from octadecyltrichlorosilane precursor molecules. On the OTS film, we fabricated the carboxylic acid-terminated chemical patterns (OTSpd) using atomic force microscope (AFM) oxidation lithography (Scheme 1a).[24−26] Next, the lysozyme pattern was fabricated on the OTSpd template (Scheme 1b). Then, we incubated the lysozyme pattern in the solution of antilysozyme aptamers to form the edge-bound aptamer structure (Scheme 1c). After the subsequent AFM characterization revealed that the edge-bound aptamer structure had formed on the lysozyme pattern, we incubated the sample in the buffer solution again to form the aptamer fibers (Scheme 1d). Finally, we used the aptamer fibers as a template to synthesize nanowires. In the first example, we incubated the aptamer fibers with a solution of palladium acetate and then reduced the Pd^{2+} bound on the fiber to form the Pd nanowires (Scheme 1e). In the second example, we fabricated aptamer fibers made of biotin-tagged antilysozyme aptamer. Then we incubated the aptamer fiber template with the streptavidin solution. The streptavidin selectively assembled on the aptamer fiber template, forming streptavidin nanowires (Scheme 1f).

Aptamers self-assembled into fibers. Previously, we found that antilysozyme aptamers biospecifically bound on the edge of a tightly packed lysozyme pattern, because lysozyme molecules on the edge of the pattern have better accessibility and flexibility than the lysozyme molecules in the interior.[23] Based on this earlier discovery, in this study we found that these edge-bound aptamer molecules served as anchors; additional aptamer molecules could self-assemble into fibers, one end of which could hinge to the edge-bound aptamer molecules. Previously we showed that if the sample was sufficiently rinsed with deionized water, the nonspecifically adsorbed aptamers on OTS would be washed off the surface, leaving a clean background.[23] We found that to reliably fabricate long aptamer fibers anchored on the lysozyme pattern's edge, the procedure has to be conducted in two steps, which is different from our previously reported procedure for the aptamer binding.

In the first step, aptamer molecules selectively bound on the lysozyme edges through incubating the sample in aqueous solution. Incubating in water instead of buffer solution precluded the assembly and precipitation of aptamers. In aqueous solution, the aptamer molecule is negatively charged, which makes it difficult to form the optimized structure for target binding. The aptamer molecules bound to target lysozyme almost immediately in a 50 mM pH 7 buffer. In contrast, in water, we found that it took 10 h for aptamer to bind on the lysozyme. We speculate that, in water, although a majority of aptamer molecules are not in the optimized structure for target binding, a variety of aptamer conformations coexist and interchange. Therefore, there is still a small fraction of aptamer molecules in the binding conformation. Given enough incubation time, the lysozyme molecules on the edge of the protein pattern will be bound by the aptamer molecules

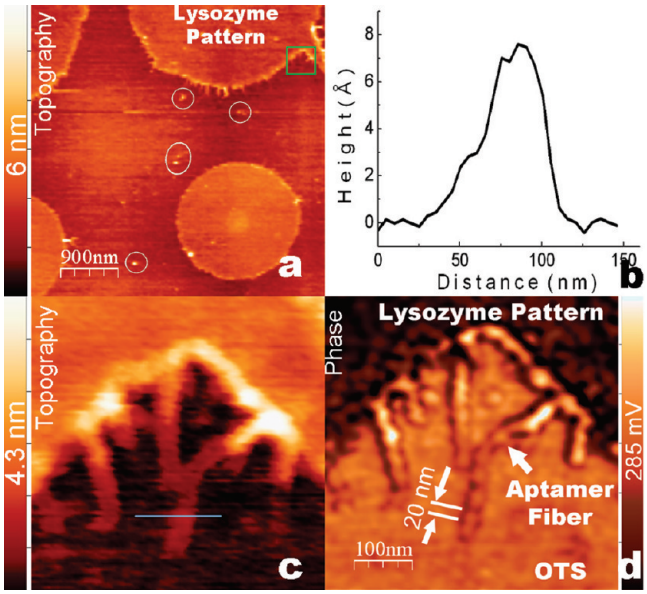

Figure 1. (a) Lysozyme patterns (disks) after incubation with antilysozyme aptamers in water: topography, 4.5 × 4.5 μm², the image was acquired using Agilent PicoPlus 3000 in AC mode. Aptamers biospecifically bound on the edge of the lysozyme disks, forming rings over the edges. Aptamers also began to self-assemble from the edge of the disks, forming short fibers. A few aggregates are also observed, as shown inside the white circles. They did not anchor on any of the edges of lysozyme disks. Aptamers also adsorb on the OTS. But due to their small size and mobile nature, they are invisible under AFM. The horizontal lines in the image were caused by interactions between these nonspecifically adsorbed aptamers on the OTS and the AFM tip. When the tip dragged them, a line was generated in the image. (b) The height cross-sectional plot corresponding to the blue line in c, showing the diameter of the fiber is 8 Å. (c,d) Topography and phase images of the region inside the green box in (a): 500 × 500 nm², AC mode; ~20 nm sized aptamer can be identified in the high-resolution phase image.

with the right structure. Figure 1a shows that the edge of the protein pattern is higher than the interior of the lysozyme disk, indicating that the antilysozyme aptamer molecules bound on top of the lysozyme molecules on the pattern edge. However, to facilitate the subsequent aptamer self-assembly, we deliberately rinsed the sample with deionized water briefly, leaving many aptamers also nonspecifically adsorbed on the OTS background. Most of these mobile aptamer molecules on OTS are invisible under AFM, because they were dragged by the AFM tip and moved with the AFM tip during the scanning. As a result, the background in Figure 1a is noisy. Horizontal lines are visible in the figure, which were caused by the interactions between weakly adsorbed aptamers on OTS and an AFM tip. Some of the aptamers also formed aggregates, which nonspecifically adsorbed on the OTS background. These aggregates are shown within the white circles in Figure 1a. Aptamer fibers 200−400 nm long also grew from the edge of the protein pattern. They are illustrated in the white box in Figure 1a. When the sample was incubated with 2 μM aptamers aqueous solution, these aptamer fibers can only grow to 200−400 nm long. Longer incubation time did not lead to the further growth of these aptamer fibers. In Figure 1c and d we show the zoom-in view of the green box in Figure 1a. Figure 1c and d are the topography image and the corresponding phase image, respectively. Both images clearly show that the short aptamer fibers grew from the edge of the lysozyme pattern. Figure 1b shows the height profile corresponding to the blue line in Figure 1c. The plot in Figure 1b indicates that the height of the aptamer fiber is 8 Å. The phase image of the aptamer fiber in Figure 1d reveals that the fiber is composed of multiple structural units with size of 20 ± 2 nm. The 42-mer double-stranded DNA would be 14 nm long and 2.2 nm in height. Assuming the base-to-base distance in a fully stretched single-stranded DNA is 7.5 Å,[27] a 42-mer single-stranded antilysozyme aptamer is 31.5 nm long when it is fully stretched. However, if aptamer molecules are linked together through the hydrogen bonding between the complementary bases on different aptamer molecules, the base-to-base distance will decrease in the hydrogen-bonded section, which makes the possible full length of the aptamer molecules smaller than the fully stretched length. On the other hand, the observed height of the fiber in Figure 1c is only 8 Å, indicating that the DNA strand is not as coiled as a double-stranded DNA. Hence, the base-to-base distance should be longer than that in double-stranded DNA. Based on these factors, we suggest that the observed periodic 20 nm sized structural unit on the aptamer fiber is the individual antilysozyme aptamer. Therefore, the AFM image in Figure 1d reveals that the fiber grown from the edge of the lysozyme pattern is the fiber formed from the assembly of antilysozyme aptamers.

In the second step, we incubated the sample in a 10 mM tris(hydroxyly)aminomethane (Tris) buffer to grow aptamer fibers up to tens of micrometers long. After the incubation, we observed the formation of

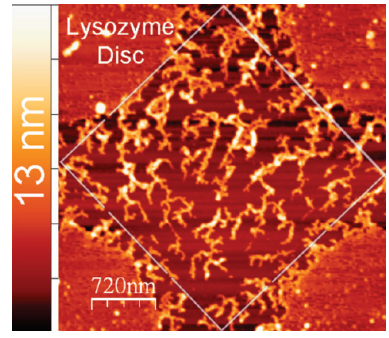

Figure 2. Branched, long aptamer fibers formed after the sample was incubated in Tris buffer: topography image, 3.6 × 3.6 μm²; AC mode.

branched, long fibers, which were formed from the nonspecifically adsorbed aptamer molecules on OTS background. Longer incubation time led to the formation of longer fibers, which were anchored on the edge of the lysozyme pattern, as shown in Figure 2. Occasionally, there were also trace amounts of isolated orphan fibers that did not anchor on the edge. These orphan fibers would disappear after additional rinsing with the buffer solution; they were either captured by other edge-anchored fibers or rinsed off the sample surface. The fiber's length is only limited by the space between the lysozyme disks, as shown in Figure 2. When most of the branches are as close as ~20 nm, the fiber stops growing. In contrast, the fiber grown in an unconfined area could reach to tens of micrometers in length. The diameter of the fiber is not even. Fibers in the terminal branches are thinner, with a typical diameter of 1−2 nm, whereas fibers in the "mainstream" have a typical diameter of 5−6 nm. These fibers adopt the fractal shape. Under our preparation conditions, different branches can be as close as 20 nm, but the fibers in one branch do not connect to fibers from other branches nor do they cross over or collapse over each other. Incubating the fibers in buffers with higher ionic concentrations (>50 mM) would slightly change the position of the fiber on the surface.

We suggested that these fibers were made of DNA.[23] Our control test showed that no fiber was generated when the lysozyme pattern was incubated in a blank Tris buffer. The fiber appeared only after the aptamer was added into the Tris buffer. The observed fibers that were several micrometers long had a 1−5 nm diameter. Because an antilysozyme aptamer molecule (42-mer) is ~20 nm long and 1−2 nm in diameter, the fibers must consist of many aptamers self-assembled together, as we had observed in Figure 1d. We speculate that the driving force of the self-assembly is the intermolecular hydrogen bond between single-stranded aptamers. To test our hypothesis, we performed control experiments with two oligonucleotides: a randomly generated single-stranded 42-mer DNA (random sample, sequence 5′-TAT GCT AAA CCT TAC AAG TTG GAA GTC GAG CGT TGA AGC AGG-3′) and a single-stranded 50-mer DNA that is composed of only the guanine (polyG). Results showed that the random sample also formed fibers on the surface, although these fibers could not anchor on the edge of the pattern. As a comparison, we did not observe any fiber formation for the polyG case. For both single-stranded DNAs that form fibers (the antilysozyme aptamer and the random sample), we found that there were complementary regions in their sequences for the interstrand base pairing (as shown in the Supporting Information, Figures S1 and S2). In contrast, the polyG was unable to find any complementary nucleotide (the cytosine) on another polyG. Therefore, no hydrogen bond existed between two polyG strands. Thus, the polyG cannot self-assemble into fibers. Furthermore, to test our hypothesis, we incubated the fibers of the antilysozyme aptamer in water at 55 °C for 10 h. The fibers disappeared from the surface after the incubation, while the protein pattern remained intact. The disappearance of the fibers can be explained by the destruction of hydrogen bonds at an elevated temperature. Therefore, the aptamers in the fiber were disassembled. Finally, to confirm the observed fibers originated from the DNA assembly, we conducted two more experiments. We incubated the fibers in deionized water for 72 h. The fibers remained intact. This fact rules out the possibility that the fiber originated from salt drying patterns, because the salt would be soluble in water and the salt pattern would disappear after incubation in water. We also stained the fiber with a 10 mM solution of ethidium bromide (EtBr), which is known to selectively bind to DNA and yields fluorescence upon excitation.[28,29] After rinsing, we imaged the same region on the sample using AFM and a fluorescent microscope. The AFM topography image (Figure 3a) and the fluorescence microscope image (Figure 3b) of the fibers matched exactly, as shown in Figure 3c. The exact matching indicates that the

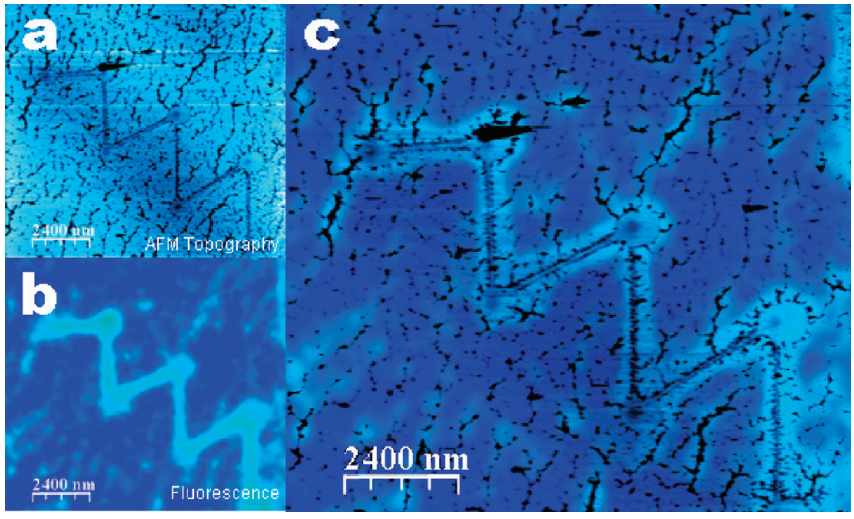

Figure 3. Fluorescent image of ethidium bromide-stained aptamer fibers (bright) matches exactly with the AFM image of aptamer fibers (black) of the same region. (a) AFM topography image of aptamer fibers grown from a zigzag-shaped lysozyme pattern. The image is rendered in the reverse height scale. Black represents high surface features, while a low surface feature corresponds to the bright color. (b) Optical fluorescent image of the same region. The fluorescent image was acquired using Nikon Eclipse N55i microscope, with the G-2A filter, which selectively collected fluorescence signal from ethidium bromide from 550−600 nm. (c) AFM and fluorescent images are overlaid together. The perfect matching indicates that the observed fibers are made of DNA, which can bind ethidium bromide. (Note: Some aptamer fibers in the AFM topography images 2a and 2c appear as broken. In fact, at higher height resolution, these fibers are continuous.)

fluorescence signal is from the fiber. Therefore, the fiber is made of DNA.

In summary, although fractal-shaped patterns may be generated from the salt drying process, the above control tests and the fiber's incubation time-dependent growth kinetics rule out the possibility of the salt-drying origin of these fibers.

Similar fiber-shaped and network-shaped structures formed by the DNA self-assembly have been reported previously.[30−32] In contrast to these previous reports, the aptamer fibers fabricated in our approach can recognize and grow from the edges of the pattern. One terminus of the fiber is bound to the edge of a pattern. Such spatial control originates from the biospecific recognition between the antilysozyme aptamer and the lysozyme molecules on the edge of the pattern. In contrast, when the lysozyme pattern was incubated with the random DNA sample, short fibers and clusters also formed. But they only nonspecifically adsorbed on the OTS background. They did not anchor on the edge of the lysozyme pattern. Therefore, the fibers formed by the random sequence have no recognition ability. After the sample was incubated in deionized water at 25 °C for 8 h and then rinsed with water three times, these nonspecifically adsorbed fibers were rinsed off the sample, leaving only the protein pattern on the surface. For the fibers formed from the antilysozyme aptamer, after such procedure, they remained because these fibers have anchors on the edge of the lysozyme pattern, where aptamers bound to the lysozyme molecules on the edge.

The diffusion-limited aggregation (DLA) theory can be used to explain the mechanism of the fiber formation.[33] Experiments and simulations have shown that DLA generates the fractal shape very similar to the observed aptamer fibers.[34−36] We observed that when aptamers reacted with the lysozyme pattern, some aptamer molecules specifically bound on the edge of the lysozyme pattern, while other aptamers nonspecifically adsorbed on the OTS background could randomly walk around the surface. The edge-bound aptamers served as seeds for the subsequent DLA process. During the Tris buffer incubation, when a mobile nonspecifically adsorbed aptamer encountered the seed, the seed captured it. Thus, a dimer was formed on the edge of the protein pattern. Similarly, when the third aptamer randomly walked into the dimer, it was captured by the dimer to form a trimer. When such process repeated, the assembly grew longer, leading to a fractal shape. There are two types of DLA. One is the classical Witten−Sander type,[33] in which only one seed exists during the growth of a branch and all particles assemble to a branch one by one. The other type is the cluster−cluster model (CL-CL), where particles (aptamers in our case) also self-assemble into small freestanding clusters.[37] Besides the mobile particle that can randomly walk on the surface, these clusters also can

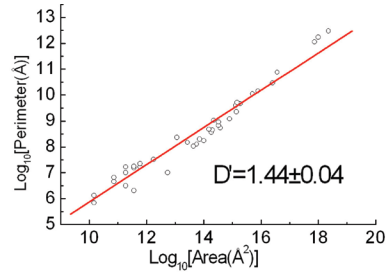

Figure 4. Aptamer fibers within the white box in Figure 2 were analyzed by the perimeter-area method to calculate the fractal dimension. The logarithm of perimeter was plotted versus the logarithm of area. The red line shows the least-squares linear fitting of the data points.

randomly walk on the surface and be captured by the edge-bound seed aptamers. The final shape formed by the CL-CL DLA is also the fractal shape. The difference between these two types of DLA is that the fractal formed by Witten−Sander type DLA is more flower-like, with a fractal dimension of 1.7 in the two-dimensional case,[34] while the fractal formed by the CL-CL DLA is more wire-like, with a fractal dimension between 1.4−1.5.[37] Because the fractal dimension reveals the mechanism of the formation of fractals, we use the perimeter-area method to calculate the dimension of the fractal formed by aptamer fibers to study how the aptamers assemble to a fiber.[38] In the perimeter-area method, the perimeter (P) and the area (A) of a fractal pattern are measured first. The P and A are related by the formula

$$P = \alpha D' A^{D'/2} \quad (1)$$

where α is a constant and D' is the fractal dimension. Therefore,

$$\log_{10} P = \frac{D'}{2} \log_{10} A + cons\tan t \quad (2)$$

Figure 2 is a representative fractal pattern formed by aptamer fibers. These fibers grew from edges of the four lysozyme disks, which are at the four corners of the image. We analyzed the aptamer fractal inside the white box in Figure 2 and plotted $\log_{10} P$ against $\log_{10} A$ of the fractal patterns in Figure 4. Eq 2 indicates that the slope of the least-squares fitting line (the red line in Figure 4) is $D'/2$. Thus, from this plot, the dimension of the aptamer fiber fractal is calculated to be 1.44 ± 0.04. This value suggests that the fiber formation is in line with the CL-CL DLA mechanism. Not only can a single aptamer randomly walk on the surface and then join to the fiber already anchored on the edge of a lysozyme pattern, but also aptamers can self-assemble into short freestanding fibers (clusters) on the OTS background, and these fibers then can randomly walk and be captured by the fibers that had already anchored from the pattern edge. In fact, AFM data also support this conclusion from the fractal analysis. When lysozyme patterns were incubated with the solution of aptam-

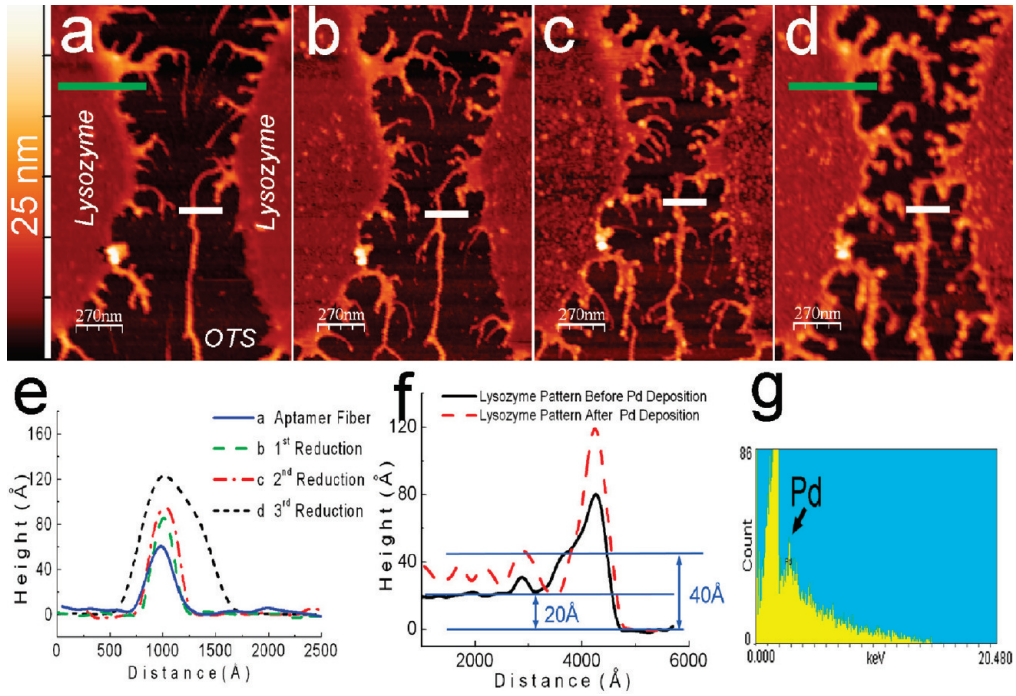

Figure 5. Aptamer fibers were converted into Pd nanowires. (a−d) The same region *before* the metallization and *after* the first, the second, and the third cycle of metallization. The height cross-sectional profiles of the same position on an aptamer fiber in (a), (b), (c), and (d) were plotted in (e). (f) Height cross-sectional profiles of the lysozyme pattern *before* the Pd deposition (black solid line) and the same place after three cycles of Pd depositions (red dash line). The black (solid) line and the red (dash) line correspond to the green bar in (a) and (d), respectively. (g) EDX spectrum of the sample. The peak at 2.8 keV confirmed the existence of Pd on the surface.

ers, after rinsing, the AFM image revealed that a small amount of isolated short fibers (aggregates) still existed. The white circles in Figure 1a show the positions of these aggregates. They are weakly adsorbed on the surface. Rigorous rinsing can minimize the presence of these freestanding aggregates from the surface. These short isolated fibers are the "clusters" under the CL-CL DLA mechanism, which might be captured by a pattern-edge-anchored fiber and thus be incorporated to form a longer fiber if the sample was incubated in the Tris buffer for a longer time.

Under the two-dimensional DLA mechanism, an aptamer molecule cannot be captured by two branches at the same time. Therefore, different aptamer fibers from two branches will never connect to each other, nor do they cross over or collapse over each other. Therefore, the mechanism provides an explanation of the AFM data, in which the aptamer fibers from different branches never connect or cross over each other.

The aptamer fibers can be used as a scaffold for the next stage assembly. As a demonstration of the application of aptamer fibers as scaffolds, we show two examples of nanowires fabricated on the aptamer template. In the first example, we fabricated Pd nanowires on the aptamer fiber template, which demonstrates a template synthesis process that is not aptamer specific. In the second case, we fabricated streptavidin nanowires on the fiber scaffold that was assembled from biotin-tagged antilysozyme aptamers, showing that the chemistry of individual aptamer can determine the template synthesis as well.

Pd Nanowires Fabrication. We fabricated Pd nanowires that anchored to the edges of a pattern. The aptamer fibers are still a structure of DNA, which can be converted to metal nanowires through DNA metallization.[39−42] Pd nanowires can be fabricated through the reduction of DNA-bound Pd^{2+}.[43−45] We conducted Pd reduction in three cycles. In the first cycle, aptamer fibers were incubated with the solution of $PdAc_2$ for 5 min. After rinsing, the sample was then soaked in the reducing solution for another 5 min. In the second cycle, the same sample was incubated in the $PdAc_2$ solution for an additional 15 min and then it was soaked in the reducing solution for 15 min. In the third cycle, we added another 15 min for $PdAc_2$ incubation and reduction, respectively. Figure 5a−d shows the same region of aptamer fibers before and after the first, second, and third cycle of the metallization process. After the reduction, most fibers maintained the basic structure and morphology. In Figure 5e, we plotted the height cross-sectional profile of the same part of an aptamer fiber *before* and *during* the metallization process. After the first, second, and third cycle of reduction, the height of the aptamer fiber increased from 60 to 90, 100, and 120 Å, respectively. Comparing the images from Figure 5a−d, there were additional fine fibrils attached to the thick palladium wires. They formed from the trace remnant nonspecifically adsorbed aptamer

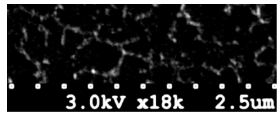

Figure 6. SEM image of Pd nanowires on the aptamer fiber template.

molecules on the OTS background. During the Pd^{2+} reduction process, the incubation process also facilitated the further assembly of these remnant nonspecifically adsorbed aptamer molecule. The fiber's full width at half-maximum (fwhm) increased from 280 Å before the metallization to 670 Å after three cycles of reduction. As shown in Figure 5a, there are also faint white spots scattering around on the lysozyme disks. These spots are the aptamer molecules bound to the lysozyme molecules inside the disk. Although the aptamer molecules preferentially bind to the lysozyme molecules on the edge, aptamer molecules can still bind to the interior lysozyme molecules during long incubation. In this image, the preferential edge-binding effect shows that the edge positions were fully occupied, whereas just a few aptamer molecules were scattered around on the lysozyme disk. However, due to the existence of these aptamer molecules inside the lysozyme disk, palladium was also selectively deposited on the lysozyme disk during the metallization. From Figure 5a−d, the images clearly show that the Pd particles accumulated on the lysozyme disk until a film of Pd nanoparticles formed on the lysozyme surface. In Figure 5f, we plotted the height cross-sectional profiles of a lysozyme disk *before* the Pd deposition and *after* the three cycles of Pd reduction. The lysozyme is 20 Å above the OTS background before the metallization, similar to our previous result.[46] After Pd reduction, the height of the disk is 40 Å above the OTS, indicating that a layer of 20 Å Pd was deposited on the lysozyme surface. The amount of palladium deposited on the lysozyme disk is much less than that on the fiber, which is due to the low density of the aptamer molecules on the lysozyme disk before the palladium deposition. Because just a few negatively charged aptamers were bound on the lysozyme disk, the amount of the Pd^{2+} bound to these aptamer molecules was insignificant. Therefore, after reduction, the Pd layer was just 20 Å thick. Figure 6 shows the scanning electron microscope image of the Pd nanowires after three cycles of reduction. The diameter of the Pd nanowire is 20−50 nm, which is consistent with the AFM results. The Pd nanowire is made of Pd nanoparticles fused together and the whole wire is continuous. These characteristics are similar to published results.[40,45,47]

In the control test, we incubated aptamer fibers with the reducing solution, but skipped the previous $PdAc_2$ incubation step. The fibers and lysozyme patterns in the control test remained the same. No changes in the fiber's width and height were observed.

We also characterized metal-coated fibers using energy-dispersive X-ray spectroscopy (EDX). EDX analyzes the composition of elements within a volume of a few cubic micrometers under the electron beam-impacted area. In the EDX spectrum shown in Figure 5g, besides an overwhelming peak of silicon, the peak at 2.8 keV confirmed the presence of Pd on the surface.

Therefore, metal nanowires that anchored on the pattern edges were fabricated. These wires are highly branched. Different branches never connect to each other. Conveniently, the lysozyme patterns were also coated by a layer of metal during the DNA metallization. Thus, the pattern can be directly used as electrodes attached with metal nanowires. These metal nanowires can be used as nanosensors and nanoelectrodes.

Fabrication of Streptavidion Nanowires on the Fiber Template Made of Biotin-Tagged Aptamer. The biotin-tagged antilysozyme aptamer was used to fabricate the branched long aptamer fiber at first. Then, after incubating the sample with streptavidin, the sample was rinsed and imaged using AFM. By comparing the same aptamer fiber before and after the incubation, we found the biotin-tagged aptamer fibers grew higher, indicating the streptavidin binding. To further test the streptavidin binding, we incubated the biotin-tagged aptamer fiber with the fluorescein isothiocyanate (FITC)-tagged streptavidin. We imaged the same region on the surface using both AFM and a fluorescence microscope. We chose the FITC-optimized filter during the fluorescence imaging. The filter blocked the fluorescent signal from DNA and only selectively collected the fluorescence signal from FITC. Figure 7a shows the AFM topography image of the fibers (black in the image) overlaid on the fluorescent image (fluorescence signal is bright). The fibers in the AFM topography image are always overlapped with bright bands in the fluorescent image, albeit the width of the bright band is about 500 nm, which approaches the diffraction limit of the optical microscopy. Figure 7a shows that the two images match exactly, indicating that the fluorescence is from the fiber. Therefore, the streptavidin indeed bound on the aptamer fibers that assembled from the biotin-tagged antilysozyme aptamer.

Figure 7c and d are the topography and phase zoom-in views of the yellow box in Figure 7a, respectively. This high-resolution AFM phase image resolves the aptamer fiber (black in the phase image) and the streptavidin molecules (bright dots on the fiber). The discrete streptavidin molecules can be resolved, as pointed by the white arrows in Figure 7c. The size of a single streptavidin tetramer in the Figure is 10 nm, which is slightly larger than the actual dimension of a streptavidin tetramer (7.3 × 8 × 4.4 nm, determined from the crystal structure).[48] We explain this difference as the tip convolution effect. Figure 7b plots the height cross-sectional profile along the blue line in Figure 7c.

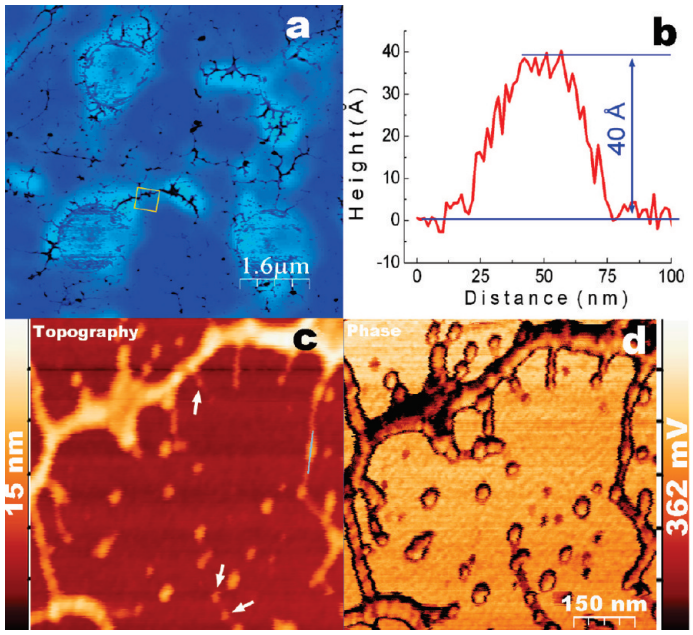

Figure 7. FITC-labeled streptavidin assembled on the biotin-tagged aptamer fibers. (a) AFM topography image of the FITC-labeled streptavidin assembled on the biotin-tagged aptamer fibers (black) overlaid on the fluorescent image (bright) of the same region. The fluorescent image was acquired using Nikon Eclipse N55i microscope, with the FITC-optimized filter, which selectively blocked the fluorescence signal from DNA. The matching of the AFM and fluorescent images indicates that FITC-labeled streptavidin molecules bind on the fibers made of biotin-tagged antilysozyme aptamer. (b) Height cross-sectional profile along the blue line in (c), showing the streptavidin molecule is 40 Å higher than the aptamer fiber template. (c,d) High-resolution AFM topography and phase images of the aptamer fibers in the yellow box in (a). The white arrows in (c) show the positions of individual streptavidin molecules bound on the aptamer fiber. (AC mode, 750 × 750 nm^2; Note: Some aptamer fibers in (a) appear as broken. In fact, at higher height resolution, these fibers are continuous.)

The plot shows that the streptavidin molecules are 4 nm above the aptamer fiber, which is consistent with the reported 3.5− 4.5 nm height values measured by AFM.[48−50] Data in Figure 7 confirm that branched, long nanowires of streptavidin were fabricated on the aptamer template, which has one end anchored on the edge of the protein pattern.

CONCLUSION

We found that aptamer molecules can form fibers up to tens of micrometers long. Unlike the *ad hoc* DNA assembly in solution, which forms DNA networks upon drying on surface, the aptamers formed long fibers *via* surface DLA process. This one-dimensional assembly approach generates long DNA wires without the need of purifying long λ-DNA or synthesizing several thousand base pair-long DNA strands.

Based on the biospecific recognition between the antilysozyme aptamer and lysozyme, we successfully fabricated nanowires that anchored on the edge of protein patterns. The biospecific recognition of the aptamer fiber controls the position of nanowires. These aptamer fibers could help to interface with other existing surface structures like DNA origamis, nanowires, electrodes, and transistors. Due to its DNA nature, additional tags, such as −SH or other aptamer, can be incorporated into the current sequence of the aptamer. Thus, the engineered fiber scaffold can be used to direct the subsequent assembly on the aptamer fiber template.

In summary, by exploiting the biospecific recognition of aptamer, we developed a new approach that improved the spatial control and interfacing capability of DNA assemblies.

EXPERIMENTAL SECTION

Materials and Instruments. Silicon (100) wafers (nitrogen doped, 5 Ω · cm resistivity) were purchased from KC electronics. The wafer was polished to the ultraflat level with a root-mean-square (rms) roughness smaller than 5 Å. Toluene, hydrogen peroxide, sulfuric acid, palladium acetate, sodium citrate, lactic acid, borane dimethylamine, and lysozyme were purchased from Sigma-Aldrich. Octadecyltrichlorosilane (OTS, 97%) was from Gelest. Antilysozyme aptamer[16,51] (sequence: 5′-ATC TAC GAA TTC ATC AGG GCT AAA GAG TGC AGA GTT ACT TAG-3′) and biotin-tagged antilysozyme aptamer (sequence: 5′-ATC TAC GAA TTC ATC AGG GCT AAA GAG TGC AGA GTT ACT TAG-biotin-3′) were obtained from Operon.

The chemical pattern fabrication and characterization were performed using Agilent PicoPlus 3000 AFM in an environmental chamber. The carboxylic acid-terminated chemical pattern (OTSpd) was fabricated in contact mode, with the MikroMasch CSC-17 Platinum−Titanium coated tip. All images were processed with WSxM.[52] The OTSpd and lysozyme patterns were characterized in AC mode with MikroMasch NSC-14 tips. The thickness and quality of the OTS film were examined with Angstrom Advanced PhE 101 laser ellipsometer and Varian Excalibur 3100 Fourier transform infrared spectrometer.[53] The resistivity of the silicon wafer was measured with a Signatone four-point probe. The Pd nanowires were characterized using a Hitachi SE-3200 scanning electron microscope (SEM) for EDX analysis. The fluorescent image of aptamer fibers and streptavidin nanowires were acquired using the Nikon fluorescence microscope N55i.

Lysozyme Pattern Fabrication. We have developed a simple way to fabricate a one-layer-thick, tightly packed lysozyme pattern on the OTSpd chemical template, which has been documented elsewhere.[46] Briefly, we used a conducting AFM tip to conduct the nanoscale electrochemical oxidation on the methyl-terminated OTS film in a 100% relative humidity (at 25 °C) environment. After a +10 V bias was applied to the sample, the methyl-terminated surface under the AFM tip was converted into a OTSpd pattern. Subsequently, the sample was incubated in a solution containing 4 μg/mL lysozyme and 10 mM 4-(2-hydroxyethyl)-1-piperazineethanesulfonic acid (HEPES, pH 7.0) buffer at 25 °C for 10 h. Lysozyme has an isoelectric point of 11.[54] Therefore, lysozyme carries positive charges in the pH 7.0 HEPES buffer, whereas the carboxylic acid-terminated OTSpd carries negative charges in the buffer. Columbic force drives the lysozyme to selectively adsorb on the OTSpd template. The sample was then rinsed with water and swabbed with Chem-Wipe paper to remove the nonspecifically adsorbed lysozyme on the OTS background.

Fabrication of Aptamer Fibers. In the first step, the lysozyme pattern was incubated in a 2 μM aqueous solution of antilysozyme aptamers for 10 h. The aptamer biospecifically and preferentially bound on the edge of the lysozyme pattern.[25] Additional aptamer molecules nonspecifically adsorbed on the OTS background. In the second step, the aptamer-loaded sample was in-

cubated in a 10 mM Tris (pH 7.0) buffer at 25 °C for 10−72 h. Then the sample was incubated and rinsed in deionized water at 25 °C. In the Tris buffer, aptamers self-assembled into fibers, which anchored on the edge of the lysozyme pattern.

Conversion of Aptamer Fibers into Pd Nanowires. We followed the established protocol for the DNA metallization.[40] Briefly, 10 mg palladium acetate was dissolved in 4 mL deionized water. After 3 min of ultrasonication, the solution was centrifuged at 9000 *g* for 5 min to remove any insoluble particles. The solution was then diluted to 30% of the original concentration. Next, the aptamer fibers were incubated with the palladium acetate solution. After rinsing the sample with water, the sample was incubated with the reducing solution (250 mg/L sodium citrate, 250 mg/L 85% lactic acid and 25 mg/L borane dimethylamine).

Fabrication of Streptavidin Nanowires on the Aptamer Fiber Template Made of Biotin-Tagged Antilysozyme Aptamer. Biotin-tagged aptamer fibers were fabricated according to the same procedure mentioned above. Then the sample was incubated in 4 μg/mL streptavidin in 25 mM pH 7.0 HEPES buffer for 1 h. Then the sample was rinsed in the 25 mM pH 7.0 HEPES buffer and deionized water before characterization.

Acknowledgment. This research is supported by the University of Kentucky faculty start-up fund.

Supporting Information Available: Analyses of the sequences of antilysozyme aptamer and the random sample. This material is available free of charge *via* the Internet at http://pubs.acs.org.

REFERENCES AND NOTES

1. Kolmakov, A.; Moskovits, M. Chemical Sensing and Catalysis by One-Dimensional Metal-Oxide Nanostructures. *Annu. Rev. Mater. Res.* **2004**, *34*, 151–180.
2. Law, M.; Greene, L. E.; Johnson, J. C.; Saykally, R.; Yang, P. D. Nanowire Dye-Sensitized Solar Cells. *Nat. Mater.* **2005**, *4*, 455–459.
3. Cui, Y.; Wei, Q. Q.; Park, H. K.; Lieber, C. M. Nanowire Nanosensors for Highly Sensitive and Selective Detection of Biological and Chemical Species. *Science* **2001**, *293*, 1289–1292.
4. Liu, H. Q.; Kameoka, J.; Czaplewski, D. A.; Craighead, H. G. Polymeric Nanowire Chemical Sensor. *Nano Lett.* **2004**, *4*, 671–675.
5. Goldberger, J.; Hochbaum, A. I.; Fan, R.; Yang, P. D. Silicon Vertically Integrated Nanowire Field Effect Transistors. *Nano Lett.* **2006**, *6*, 973–977.
6. Martensson, T.; Carlberg, P.; Borgstrom, M.; Montelius, L.; Seifert, W.; Samuelson, L. Nanowire Arrays Defined by Nanoimprint Lithography. *Nano Lett.* **2004**, *4*, 699–702.
7. Menke, E. J.; Thompson, M. A.; Xiang, C.; Yang, L. C.; Penner, R. M. Lithographically Patterned Nanowire Electrodeposition. *Nat. Mater.* **2006**, *5*, 914–919.
8. Sun, Y. G.; Khang, D. Y.; Hua, F.; Hurley, K.; Nuzzo, R. G.; Rogers, J. A. Photolithographic Route to the Fabrication of Micro/Nanowires of III-V Semiconductors. *Adv. Funct. Mater.* **2005**, *15*, 30–40.
9. Lu, W.; Lieber, C. M. Nanoelectronics from the Bottom Up. *Nat. Mater.* **2007**, *6*, 841–850.
10. Seeman, N. C. DNA in a Material World. *Nature* **2003**, *421*, 427–431.
11. Yan, H.; Park, S. H.; Finkelstein, G.; Reif, J. H.; LaBean, T. H. DNA-Templated Self-Assembly of Protein Arrays and Highly Conductive Nanowires. *Science* **2003**, *301*, 1882–1884.
12. Simmel, F. C.; Dittmer, W. U. DNA Nanodevices. *Small* **2005**, *1*, 284–299.
13. Friedrichs, E.; Simmel, F. C. Controlling DNA Polymerization with a Switchable Aptamer. *ChemBioChem* **2007**, *8*, 1662–1666.
14. Ellington, A. D.; Szostak, J. W. In Vitro Selection of RNA Molecules That Bind Specific Ligands. *Nature* **1990**, *346*, 818–822.
15. Tuerk, C.; Gold, L. Systematic Evolution of Ligands by Exponential Enrichment—RNA Ligands to Bacteriophage-T4 DNA-Polymerase. *Science* **1990**, *249*, 505–510.
16. Kirby, R.; Cho, E. J.; Gehrke, B.; Bayer, T.; Park, Y. S.; Neikirk, D. P.; McDevitt, J. T.; Ellington, A. D. Aptamer-Based Sensor Arrays for the Detection and Quantitation of Proteins. *Anal. Chem.* **2004**, *76*, 4066–4075.
17. Willner, I.; Zayats, M. Electronic Aptamer-Based Sensors. *Angew. Chem., Int. Ed.* **2007**, *46*, 6408–6418.
18. Nutiu, R.; Li, Y. F. Structure-Switching Signaling Aptamers. *J. Am. Chem. Soc.* **2003**, *125*, 4771–4778.
19. Navani, N. K.; Li, Y. F. Nucleic Acid Aptamers and Enzymes as Sensors. *Curr. Opin. Chem. Biol.* **2006**, *10*, 272–281.
20. Liss, M.; Petersen, B.; Wolf, H.; Prohaska, E. An Aptamer-Based Quartz Crystal Protein Biosensor. *Anal. Chem.* **2002**, *74*, 4488–4495.
21. Chhabra, R.; Sharma, J.; Ke, Y. G.; Liu, Y.; Rinker, S.; Lindsay, S.; Yan, H. Spatially Addressable Multiprotein Nanoarrays Templated by Aptamer-Tagged DNA Nanoarchitectures. *J. Am. Chem. Soc.* **2007**, *129*, 10304–10305.
22. Liu, Y.; Lin, C. X.; Li, H. Y.; Yan, H. Protein Nanoarrays—Aptamer-Directed Self-Assembly of Protein Arrays on a DNA Nanostructure. *Angew. Chem., Int. Ed.* **2005**, *44*, 4333–4338.
23. Gao, P.; Cai, Y. G. Label-Free Detection of the Aptamer Binding on Protein Patterns Using Kelvin Probe Force Microscopy (KPFM). *Anal. Bioanal. Chem.* **2009**, *394*, 207–214.
24. Maoz, R.; Cohen, S. R.; Sagiv, J. Nanoelectrochemical Patterning of Monolayer Surfaces: Toward Spatially Defined Self-Assembly of Nanostructures. *Adv. Mater.* **1999**, *11*, 55–61.
25. Gao, P.; Cai, Y. G. The Boundary Molecules in a Lysozyme Pattern Exhibit Preferential Antibody Binding. *Langmuir* **2008**, *24*, 10334–10339.
26. Cai, Y. G. The Partially Degraded Hydrophilic Silane Pattern and Its Application in Studying the Structures of Long Chain Alkane Films. *Langmuir* **2009**, *25*, 5594–5601.
27. Smith, S. B.; Cui, Y. J.; Bustamante, C. Overstretching B-DNA: The Elastic Response of Individual Double-Stranded and Single-Stranded DNA Molecules. *Science* **1996**, *271*, 795–799.
28. Waring, M. J. Complex Formation between Ethidium Bromide and Nucleic Acids. *J. Mol. Biol.* **1965**, *13*, 269–282.
29. Lepecq, J. B.; Paoletti, C. A Fluorescent Complex between Ethidium Bromide and Nucleic Acids—Physical−Chemical Characterization. *J. Mol. Biol.* **1967**, *27*, 87–106.
30. Aldaye, F. A.; Sleiman, H. F. Guest-Mediated Access to a Single DNA Nanostructure from a Library of Multiple Assemblies. *J. Am. Chem. Soc.* **2007**, *129*, 10070–10071.
31. Li, Y. G.; Tseng, Y. D.; Kwon, S. Y.; D'Espaux, L.; Bunch, J. S.; McEuen, P. L.; Luo, D. Controlled Assembly of Dendrimer-Like DNA. *Nat. Mater.* **2004**, *3*, 38–42.
32. Balint, Z.; Nagy, K.; Laczko, I.; Bottka, S.; Vegh, G. A.; Szegletes, Z.; Varo, G. Adsorption and Self-Assembly of Oligodeoxynucleotides Ontoa Mica Surface. *J. Phys. Chem. C* **2007**, *111*, 17032–17037.
33. Witten, T. A.; Sander, L. M. Diffusion-Limited Aggregation, a Kinetic Critical Phenomenon. *Phys. Rev. Lett.* **1981**, *47*, 1400–1403.
34. Hurd, A. J.; Schaefer, D. W. Diffusion-Limited Aggregation in Two Dimensions. *Phys. Rev. Lett.* **1985**, *54*, 1043–1046.
35. Xiao, L. H.; Zhou, R.; He, Y.; Li, Y. J.; Yeung, E. S. Direct Observation of Nanoparticle Self-Assembly Dynamics at the Water−Air Interface Using Differential Interference Contrast Microscopy. *J. Phys. Chem. C* **2009**, *113*, 1209–1216.
36. Roder, H.; Hahn, E.; Brune, H.; Bucher, J. P.; Kern, K. Building One-Dimensional and Two-Dimensional Nanostructures by Diffusion-Controlled Aggregation at Surfaces. *Nature* **1993**, *366*, 141–143.
37. Meakin, P. Formation of Fractal Clusters and Networks by Irreversible Diffusion-Limited Aggregation. *Phys. Rev. Lett.* **1983**, *51*, 1119–1122.
38. Gomezrodriguez, J. M.; Baro, A. M.; Vazquez, L.; Salvarezza, R. C.; Vara, J. M.; Arvia, A. J. Fractal Surfaces of Gold and Platinum Electrodeposits—Dimensionality Determination

by Scanning Tunneling Microscopy. *J. Phys. Chem.* **1992**, *96*, 347–350.
39. Samson, J.; Varotto, A.; Nahirney, P. C.; Toschi, A.; Piscopo, I.; Drain, C. M. Fabrication of Metal Nanoparticles Using Toroidal Plasmid DNA as a Sacrificial Mold. *ACS Nano* **2009**, *3*, 339–344.
40. Deng, Z. X.; Mao, C. D. DNA-Templated Fabrication of 1D Parallel and 2D Crossed Metallic Nanowire Arrays. *Nano Lett.* **2003**, *3*, 1545–1548.
41. Gu, Q.; Cheng, C. D.; Gonela, R.; Suryanarayanan, S.; Anabathula, S.; Dai, K.; Haynie, D. T. DNA Nanowire Fabrication. *Nanotechnology* **2006**, *17*, R14–R25.
42. Stoltenberg, R. M.; Woolley, A. T. DNA-Templated Nanowire Fabrication. *Biomed. Microdevices* **2004**, *6*, 105–111.
43. Richter, J. Metallization of DNA. *Physica E* **2003**, *16*, 157–173.
44. Richter, J.; Mertig, M.; Pompe, W.; Vinzelberg, H. Low-Temperature Resistance of DNA-Templated Nanowires. *Appl. Phys. A* **2002**, *74*, 725–728.
45. Richter, J.; Seidel, R.; Kirsch, R.; Mertig, M.; Pompe, W.; Plaschke, J.; Schackert, H. K. Nanoscale Palladium Metallization of DNA. *Adv. Mater.* **2000**, *12*, 507–510.
46. Gao, P.; Cai, Y. A Method for Fabricating Protein Patterns on the Octadecyltrichlorosialne (OTS) Surface through Paper Swabbing. *Ultramicroscopy* **2009**, *109*, 1023–1028.
47. Braun, E.; Eichen, Y.; Sivan, U.; Ben-Yoseph, G. DNA-Templated Assembly and Electrode Attachment of a Conducting Silver Wire. *Nature* **1998**, *391*, 775–778.
48. Livnah, O.; Bayer, E. A.; Wilchek, M.; Sussman, J. L. Three-Dimensional Structures of Avidin and the Avidin-Biotin Complex. *Proc. Natl. Acad. Sci. U.S.A.* **1993**, *90*, 5076–5080.
49. Leung, C.; Kinns, H.; Hoogenboom, B. W.; Howorka, S.; Mesquida, P. Imaging Surface Charges of Individual Biomolecules. *Nano Lett.* **2009**, *9*, 2769–2773.
50. Park, S. H.; Yin, P.; Liu, Y.; Reif, J. H.; LaBean, T. H.; Yan, H. Programmable DNA Self-Assemblies for Nanoscale Organization of Ligands and Proteins. *Nano Lett.* **2005**, *5*, 729–733.
51. Cheng, A. K. H.; Ge, B.; Yu, H. Z. Aptamer-Based Biosensors for Label-Free Voltammetric Detection of Lysozyme. *Anal. Chem.* **2007**, *79*, 5158–5164.
52. Horcas, I.; Fernandez, R.; Gomez-Rodriguez, J. M.; Colchero, J.; Gomez-Herrero, J.; Baro, A. M. Wsxm: A Software for Scanning Probe Microscopy and a Tool for Nanotechnology. *Rev. Sci. Instrum.* **2007**, *78*, 013705−1−013705−8.
53. Maoz, R.; Sagiv, J.; Degenhardt, D.; Miihwald, H.; Quint, P. Hydrogen-Bonded Muttilayers of Self-Assembling Silanes: Structure Elucidation by Combined Fourier Transform Infra-Red Spectroscopy and X-Ray Scattering Techniques. *Supramol. Sci.* **1995**, *2*, 9–24.
54. Koehler, J. A.; Ulbricht, M.; Belfort, G. Intermolecular Forces between Proteins and Polymer Films with Relevance to Filtration. *Langmuir* **1997**, *13*, 4162–4171.